Synthesis and Photocatalytic Degradation of Azithromycin by Iron/Zinc Oxide Nanoparticle-Reinforced Carbon Nanofibers

Poorya Hosseinabadi
University of Birjand
Mohammad Reza Rezaei
University of Birjand
Mohammad Hossein Sayadi
mh_sayadi@uk.ac.ir
Shahid Bahonar University of Kerman
Hossein Barani
University of Birjand

Article

Keywords: Azithromycin, Reactive oxygen species, Diffuse Reflectance Spectroscopy, COVID-19, Drinking water, Nanofiber

Posted Date: June 17th, 2025

DOI: https://doi.org/10.21203/rs.3.rs-6844291/v1

Additional Declarations: No competing interests reported.

Version of Record: A version of this preprint was published at Scientific Reports on August 25th, 2025.
See the published version at https://doi.org/10.1038/s41598-025-16849-x.

Synthesis and Photocatalytic Degradation of Azithromycin by Iron/Zinc Oxide Nanoparticle-Reinforced Carbon Nanofibers

Poorya Hosseinabadi[a], Mohammad Reza Rezaei[a], Mohammad Hossein Sayadi[b]*, Hossein Barani[c]

[a] Department of Environmental Engineering, Faculty of Natural Resources and Environment, University of Birjand, Birjand, Iran
[b] Faculty of Natural Resources and Environment, Shahid Bahonar University of Kerman, Kerman 7616913439, Iran.
[c] Department of Carpet, Faculty of Art, University of Birjand, Birjand, Iran

*Correspondence: mh_sayadi@uk.ac.ir

Abstract

Water pollution caused by persistent pharmaceutical contaminants, such as azithromycin, presents serious public health and environmental challenges. This study introduces iron/zinc oxide-reinforced carbon nanofibers synthesized via a scalable electrospinning process as a novel solution for treating pharmaceutical waste streams. The synthesized nanofibers showed a crystalline structure, an optimized bandgap energy of 2.899 eV, and an impressive surface area of 554 m²/g, as confirmed by XRD, Raman, and DRS analyses. Their synergistic photocatalytic activity arises from the effective integration of iron/zinc oxide nanoparticles into the carbon nanofiber matrix. Key parameters influencing azithromycin degradation including pH, reaction time, catalyst concentration, and pollutant concentration were systematically optimized. Under optimal conditions (pH 4, 27.1 mg/L catalyst dose, 15.8 mg/L azithromycin concentration), the nanofibers achieved a remarkable 97.5% degradation of azithromycin within 103 min under UV irradiation. The study further proved the photocatalyst's versatility, achieving degradation efficiencies of 98% under UV light and up to 85% under visible light, highlighting its ability to utilize diverse light sources. The reusability testing over five consecutive cycles revealed that the Fe/Zn-CNFs maintained over 80% degradation efficiency in the final cycle, underscoring their excellent stability and practical applicability. Beyond photocatalytic efficiency, the nanofibers exhibited notable antibacterial activity against *Escherichia coli* and *Staphylococcus aureus*, which can be attributed to the generation of reactive oxygen species (ROS). These results underscore the potential of iron/zinc oxide-reinforced carbon as a sustainable and effective photocatalyst for treating antibiotic-contaminated wastewater, offering a viable approach to modifying environmental antibiotic resistance.

Key words: Azithromycin, Reactive oxygen species, Diffuse Reflectance Spectroscopy, COVID-19, Drinking water, Nanofiber

Introduction

The presence of pharmaceutical pollutants in water systems poses significant environmental challenges, particularly due to the accumulation of antibiotics, such as azithromycin, an azalide subclass of macrolides (Polianciuc et al. 2020). The extensive use of antibiotics in both human and veterinary medicine has led to their accumulation in various aquatic environments, including rivers, lakes, and wastewater treatment facilities (Sosa-Hernández et al. 2021; Ortúzar et al. 2022; Munzhelele et al.

2024). Effluents from pharmaceutical facilities frequently contain elevated levels of azithromycin (Al-Hakkani et al. 2022), disrupting the natural physicochemical balance of ecosystems and contributing to the proliferation of antibiotic-resistant bacteria (Milaković et al. 2019). Due to its significant resilience to biodegradation, azithromycin is particularly difficult to remove from wastewater, and conventional biological treatment methods often fall short of complete elimination (Zheng et al. 2022).

To reduce the effects of these pollutants and ensure safe water supplies for future generations, innovative treatment techniques are essential (Khan et al. 2024). One promising approach is photocatalysis, which effectively degrades pharmaceutical contaminants like azithromycin by generating reactive species that break down complex organic molecules, thus addressing environmental contamination (Kaswan and Kaur 2023). Among the various photocatalysts, Zinc Oxide (ZnO) stands out due to its advantageous properties, making it a preferred choice for environmental remediation (Chen et al. 2017). However, ZnO's reliance on UV light limits its practical effectiveness; therefore, extending its activation to the visible spectrum is crucial for maximizing its potential in sustainably degrading pharmaceutical and organic pollutants in water systems (Godin et al. 2018; Fiszka Borzyszkowska et al. 2022; Navidpour et al. 2023).

The photocatalytic efficiency of ZnO can be significantly enhanced through iron (Fe) doping, which improves electron-hole separation and boosts light absorption (Fiszka Borzyszkowska et al. 2022). This modification enhances ZnO's photocatalytic properties and addresses serious environmental issues related to pharmaceutical contaminants in water systems (Kayaci et al. 2014; Godin et al. 2018; Dharmana et al. 2023). Numerous studies have confirmed the effectiveness of metal-doped ZnO in photocatalysis. For instance, Fe/Sn-doped ZnO microspheres exhibited reduced electron-hole recombination and improved visible light absorption, leading to enhanced photodegradation efficiency of pollutants such as ciprofloxacin and methylene blue (Song et al. 2019). Additionally, Fe-doped ZnO nanofibers demonstrated an 87% increase in pollutant degradation efficiency under sunlight compared to undoped ZnO, highlighting the significant enhancement in photocatalytic activity achieved through doping (Ranathunga et al. 2024). Research on Fe/ZnO/SiO_2 nanoparticles also indicated successful degradation of methylene blue in the presence of light, attributed to reduced band gap energy from Fe incorporation (Mohamed et al. 2012). Furthermore, Sayadi et al (2019) demonstrated that the nanocomposite GO@Fe_3O_4/ZnO/SnO_2 could degrade approximately 90.06% of azithromycin under optimal conditions, specifically at pH 3, with a reaction time of 120 min and a catalyst concentration of 1 g/L when exposed to UV light.

Carbon nanofibers (CNFs), with their high surface area, strong mechanical properties, and excellent conductivity, present an ideal support material for photocatalysts, further enhancing the efficiency of pollutant degradation in environmental remediation (Pant et al. 2021; Yao et al. 2023). The integration of CNFs with metal-doped ZnO represents a promising strategy for improving photocatalytic performance in the degradation of pharmaceutical contaminants like azithromycin.

This study aimed to identify novel applications of carbon nanofibers reinforced with iron/zinc oxide nanoparticles for the photocatalytic degradation of azithromycin in aqueous solutions. Given the limited existing research on using nanofiber substrates for degrading this antibiotic, our investigation looked-for to fill this gap by leveraging the unique properties of the nanofibrous composites. The combination of carbon nanofibers with iron and zinc oxide nanoparticles not only enhanced the dispersion and stability of the catalysts but also improved charge separation and pollutant accessibility. These advances are expected to significantly increase the efficiency of azithromycin degradation, particularly under natural sunlight conditions. By developing and characterizing these nanofiber-supported Fe/ZnO composites, we aimed to provide a promising and effective solution for tackling pharmaceutical pollution, contributing to the broader goal of ensuring cleaner water systems and reducing environmental impacts.

2. Materials and Methods

2.1. Materials

Azithromycin ($C_{38}H_{72}N_2O_{12}$) was purchased from Mascot Health Co., Ltd. Polyvinylpyrrolidone (PVP, K30, Mw = 44,000-54,000), Zinc nitrate (tetrahydrate, $Zn(NO_3)_2 .4H_2O$), Ferric nitrate (nonahydrate, $Fe(NO_3)_3.9H_2O$), Sodium hydroxide (NaOH, 96.0%), Hydrochloric acid (HCl, 37%), Anhydrous ethanol (C_2H_5OH, 99.7%), Sodium sulphate (Na_2SO_4, 99%), and Muller-Hinton (MH) agar were procured from Merck and Sigma-Aldrich. The mentioned materials were used without any purification or preliminary treatment.

2.2. Fabrication of Fe/Zn-carbon nanofibers

To prepare electrospun fibers, two solutions were prepared with 5 wt% Iron nitrate/Zinc nitrate and 40 wt% polyvinylpyrrolidone (PVP) at molar ratios of 2:1 and 1:2 for the metal salts. For the Fe:Zn solution with a 2:1 ratio, 0.0528 g of iron nitrate and 0.0171 g of zinc nitrate were dissolved in 1.87 ml of absolute ethanol and stirred for 12 h at 45°C. Then, 1.33 g of PVP was added, and the solution was stirred for an additional 24 h to prepare it for electrospinning. Similarly, for the 1:2 Fe:Zn solution, 0.0305 g of iron nitrate and 0.0394 g of zinc nitrate were dissolved in 1.87 ml of ethanol, followed by the addition of 1.33 g of PVP. After stirring for 24 h, the final electrospinning solution was obtained (Xiea et al., 2021) The electrospinning process was conducted using the settings outlined in our previous study (Barani et al. 2020). The polymer solution was fed into a needle with an inner diameter of 0.4 mm at a rate of 0.3 mL/h using a digitally controlled syringe pump. The needle was spaced 15 cm apart and charged with an applied voltage of 13.5 kV using a DC high-voltage power supply. The collector unit is a 20 cm ×15 cm flat plate (Wang et al. 2022). To ensure complete solvent (ethanol) evaporation, the electrospun fibers were removed from the aluminum sheet's surface and subjected to a vacuum oven at 180°C for 90 min. Subsequently, for annealing, the electrospun fibers were placed in an electric furnace and subjected to a specific time-temperature profile (ramping from room temperature to 800°C and holding at this temperature for 30 min). This process facilitated the degradation of PVP within the

fiber structure and crystalline phase formation, resulting in the fabrication of Fe/Zn-carbon nanofibers (Fe/Zn-CNFs) with photocatalytic activity (Lin et al. 2019). The fabrication procedure of Fe/Zn carbon nanofibers is illustrated in Fig. 1.

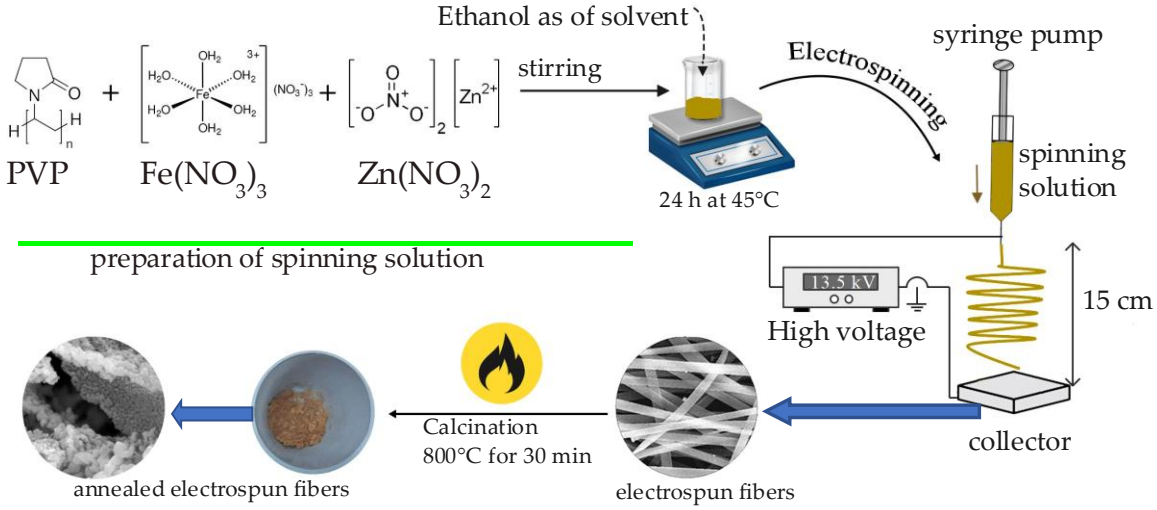

Fig. 1. Schematic representation of the fabrication process for Fe/Zn carbon nanofibers via electrospinning, including solution preparation, electrospinning parameters, and calcination process

2.3. Characterizations

Field Emission Scanning Electron Microscopy (FESEM, TESCAN MIRA2, TESCAN Company) and Energy-Dispersive X-Ray Spectroscopy (EDS) were used to examine the Fe/Zn-carbon nanofibers. Thermogravimetric analysis (TGA) was performed under Argon atmospheric conditions at temperatures ranging from 40°C to 1000°C, with a heating rate of 20°C min^{-1} (Q600, TA Company). X-ray diffraction (XRD) examination was performed on crystalline structures using an X-ray diffractometer (Philips PW 1730), with data collected ranging 10° to 80°. The chemical structure of Fe/Zn-CNFs within the range of 500-3500 cm^{-1} was characterized using a Raman spectrometer (Teksan company, model: Takram P50C0R10, Iran). Surface area analysis was conducted using a BELSORP Mini II surface area analyzer (BELSORP Company), which provided Brunauer-Emmett-Teller (BET) adsorption and desorption isotherms. The zeta potential and dynamic light scattering (DLS) of Fe/Zn-CNFs were assessed using a Malvern Zetasizer Nano ZS ZEN3600 (Malvern Instruments Limited, Worcestershire, UK). The photocatalytic activity of the samples was assessed using an ultraviolet-visible spectrophotometer (Bio Spec-1601, Shimadzu Co., Japan).

2.4. Assessment of the photocatalytic degradation of Azithromycin

In this study, a Box-Behnken response surface design was employed to optimize the photocatalytic degradation of azithromycin using Fe/Zn-CNFs. The independent variables were pH, reaction time, catalyst concentration, and azithromycin concentration. Table S1 outlines the levels of these variables.

The experimental design consisted of 30 randomized runs, including 2 center points. The selection of pH, reaction time, catalyst concentration, and pollutant concentration aimed to comprehend the fundamental aspects of photocatalytic degradation, optimize the process, and assess the potential of the proposed catalyst for modifying water pollution caused by pharmaceutical contaminants, such as azithromycin (Marinho et al. 2022).

The photocatalytic degradation experiments were conducted in a 100-mL Pyrex reactor with a cylindrical structure under UV-C light (6 W, Philips, 254 nm spectrum) at room temperature. After determining the parameter values for each experimental run, the required azithromycin solution was prepared using a 1000 mg/L stock solution. The azithromycin concentrations were quantified using an absorption peak at a characteristic wavelength of 462 nm via UV-Vis spectroscopy (Jayanna et al. 2012), based on the calibration curve and spectra of azithromycin solutions (S2).

The photocatalytic degradation efficiency of azithromycin was calculated using Equation 1:

$$\text{Efficiency}\ (\%) = \frac{C_0 - C_e}{C_0} \times 100 \quad (1)$$

In this equation, C_0 represents the initial azithromycin concentration, C_e is the azithromycin concentration after light irradiation, and Efficiency (%) quantifies the percentage of photocatalytic degradation (Karimi et al. 2014). Finally, optimization was run to obtain the highest photocatalytic degradation efficiency of azithromycin. The photocatalytic degradation efficiency of azithromycin at the optimized condition was evaluated under three different conditions: UV-C light, visible light and dark conditions.

In addition, the ability of the synthesized Fe/Zn-reinforced carbon nanofibers (Fe/Zn-CNFs) to degrade azithromycin was tested over five repeated reuse cycles under optimal conditions. To assess reusability, the photocatalyst was recovered after each cycle using an external magnetic field, ensuring minimal catalyst loss during the separation process. The recovered Fe/Zn-CNFs were then thoroughly washed multiple times with distilled water to remove any adsorbed reaction byproducts or residual pollutants and dried in an oven at 60°C for 1 h before reuse.

2.5. Kinetics analysis

Studies often use decomposition kinetics to investigate the photocatalytic degradation of a various organic compounds, particularly antibiotics. In this context, the following equation was utilized to analyze the kinetics of the azithromycin degradation reaction in the presence of Fe/Zn-CNFs (Chavoshan et al. 2020).

$$\frac{dc}{dt} = -kC \quad (2)$$

Integrating equation (2) yields equation (3):

$$\ln\left(\frac{C}{C_0}\right) = -kt \quad (3)$$

Here, in the equation, "k" represents the constant reaction rate, "t" denotes time, "C" signifies the concentration of the reactant at time "t" and "C_0" indicates the initial concentration of the reactant at time t = 0 (Golrizkhatami et al. 2023).

2.6. Antibacterial activity of Fe/Zn-CNFs

This study focused on the antibacterial properties of the prepared nanofibers**.** The Zone of Inhibition methodology was employed to evaluate this feature in accordance with the AATCC 100-2004 standard. The antibacterial properties of synthesized nanofibers have been investigated against two distinct microbial strains, *Escherichia coli* and *Staphylococcus aureus* (Morejon and Michel 2023). To prepare an appropriate culture medium for the bacteria**,** Mueller-Hinton agar medium was used (Murray and Zeitinger 1983). Bacterial strains of *Escherichia coli* (ATCC: 25922) and *Staphylococcus aureus* (ATCC: 6538) were procured in lyophilized form from the Pasteur Institute of Iran and subsequently cultured in the laboratory using the streaking method onto Petri dishes containing agar medium. The cultured bacteria were then incubated in an incubator (L.M100, Pars Azma Co.) for 48 h at 37°C. The slices of prepared nanofiber web (diameter around 1 cm) were placed onto the surface of the sterile Mueller-Hinton agar plates previously seeded with 100 µL of the bacterial suspension (1.5×10^8 CFU/mL). The plates were then incubated for 24 h at 37 °C. The antibacterial activity was determined by measuring the inhibition zones around the samples in triplicate, ensuring the reliability and reproducibility of the data.

3. Results and discussion

3.1. Morphology of electrospun fibers

The SEM images of the electrospun fibres (Fig. 2), along with their average diameter values in relation to the Fe:Zn molar ratio, demonstrate that the electrospinning process produced fibres with smooth surfaces and no bead formation. Additionally, the electrospun fibres displayed a uniform distribution of zinc nitrate and ferric nitrate with agglomerated nanoparticles visible on their surfaces after the annealing process. The sample containing Fe:Zn in the electrospinning solution with a molar ratio of 2:1 resulted in a 32% reduction in fibres diameter (from 370 nm to 250 nm) compared with the sample with a molar ratio of 1:2. This reduction can be attributed to the increased conductivity resulting from the incorporation of Fe:Zn into the spinning solution. The annealing process led to the fracturing and crushing of the nanofibers because of the removal of organic constituents and the formation of a more durable mineral phase. The synthesized nanoparticles had average sizes of 53 nm and 85 nm, corresponding to Fe/Zn molar ratios of 1:2 and 2:1, respectively. EDS analysis was employed to identify the constituents of the targeted specimen. The annealing process resulted in the appearance of distinct peaks in the EDS spectrum associated with Fe, Zn, and O, highlighting the transformative effect of annealing on the fibre's elemental composition. This transformation can be attributed to the impact of

temperature on the morphology and crystal orientation of the catalysts (Song et al. 2020; Lambora and Bhardwaj 2023).

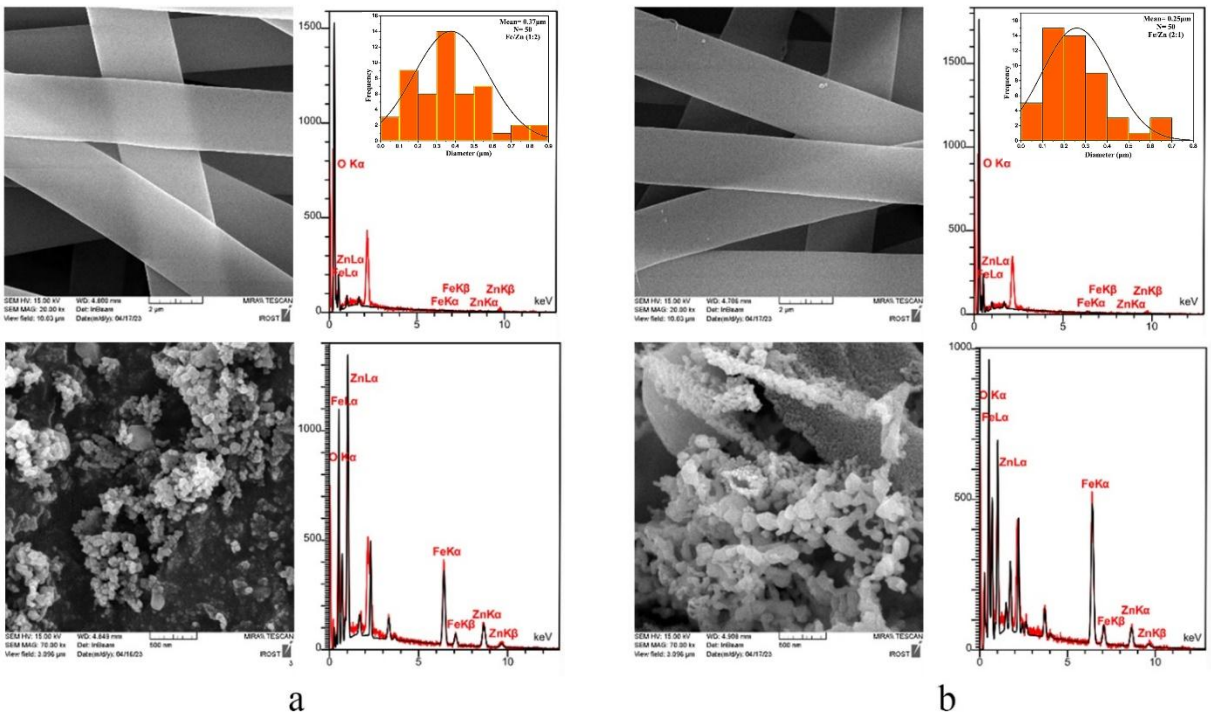

Fig. 2. Morphological analysis and EDS spectra of synthesized electrospun fibers with Fe:Zn molar ratios of 1:2 (a) and 2:1 (b) before (top) and after (bottom) annealing. The inserted histogram presents the fiber diameter distribution.

3.2. Characteristics of Fe/Zn-CNFs

The X-ray diffraction (XRD) pattern provides insight into the structural and crystalline properties of Fe/Zn nanoparticles-reinforced carbon nanofibers. In the sample with a 1:2 Fe:Zn molar ratio (Fig. 3a), significant diffraction peaks corresponding to 2θ angles of 18.15°, 29.86°, 31.73°, 34.42°, 35.17°, 36.22°, 36.79°, 42.73°, 47.51°, 53.01°, 56.50°, 56.53°, 62.03°, 62.83°, 69.01°, 70.35°, 72.56°, and 73.36° aligned precisely with crystallographic planes (111), (022), (010), (002), (113), (011), (222), (004), (012), (224), (115), (110), (044), (013), (021), (026), (004), and (335). Similarly, in the sample with a 2:1 Fe:Zn molar ratio, distinctive diffraction peaks corresponding to 2θ values of 18.38°, 30.25°, 35.63°, 37.27°, 43.30°, 53.73°, 57.28°, 62.91°, 66.15°, 71.38°, and 74.44° align with crystallographic planes (111), (022), (113), (222), (004), (224), (115), (044), (135), (026), and (335), respectively. These results corroborate the JCPDS card data (nos.96-900-2489, 96-900-4180, 96-101-0370, and 96-101-0131) and confirm the successful synthesis of Fe/ZnO nanoparticles in the prepared samples.

The variation in the XRD patterns of iron and zinc at certain angles may arise from a combination of factors, such as differences in crystalline, composition, and the Fe to Zn molar ratio. In mixed samples,

varying the Fe/Zn molar ratio in the nanofibers can influence the overall crystalline structure, lattice parameters, and peak intensities (Navidpour et al. 2023). Fe/ZnO nanoparticles exhibit a cubic crystal structure with lattice parameters of a = b = c = 8.38 Å. The nanocrystallite size, calculated from the XRD peak at 2θ = 35° using the Debye-Scherrer equation, was found to be 19 nm for the 1:2 Fe/Zn sample and 25 nm for the 2:1 Fe/Zn sample.

The UV-Vis absorption spectra of Fe/Zn (1:2) and Fe/Zn (2:1) photocatalysts, recorded using diffuse reflectance spectroscopy (DRS), are shown in Fig. 3b. The spectra reveal significant light absorption within the 300–500 nm wavelength range, indicating the photocatalysts' potential effectiveness under both UV and visible light. Notably, the absorption spectra exhibit distinct shifts, which can be attributed to iron doping.

To determine the band gap energy (E_g), the Tauc plot method was applied using the following equation (Sayadi et al. 2021):

$$(\alpha h\nu)^n = A(h\nu - Eg) \quad (4)$$

where E_g represents the band gap energy, hν is the photon energy, α is the absorption coefficient, n = 2 for direct band gap materials, and A is a constant related to material properties (Hu et al. 2015). The band gap energies of Fe/Zn (1:2) and Fe/Zn (2:1) nanofibers were calculated to be approximately 2.899 eV and 3.059 eV, respectively (the inset graph in Fig. 3b). These values are consistent with previously reported findings (Bakina et al. 2022). Pure ZnO typically has a band gap of 3.2–3.7 eV (Alam et al. 2018; Alharshan et al. 2023). However, iron doping reduced the band gap to 2.899 eV for Fe/Zn (1:2) and 3.059 eV for Fe/Zn (2:1). This red shift in the absorption spectra is attributed to interactions between the localized dd-electrons of Fe^{3+} ions and the sp−d orbitals of ZnO. The Low Eg value increases the photocatalytic activity of ZnO by shifting its maximum absorption wavelength to longer wavelengths, thereby enhancing its effectiveness under visible light. A narrower band gap facilitates the separation of photogenerated electron-hole pairs, reducing recombination and promoting efficient charge transfer. This is crucial for generating reactive species, such as hydroxyl radicals, which play key role in pollutant degradation. Iron-doped ZnO, particularly the Fe/Zn (1:2) sample, exhibiting a narrower band gap and extended absorption in the visible region, demonstrates superior potential for photocatalytic applications. For instance, it can efficiently degrade pharmaceutical pollutants like azithromycin under visible light, offering a sustainable solution for water treatment. The ability to tailor the band gap and optical properties through iron doping provides a versatile platform for designing advanced photocatalysts that harness sunlight as an economical energy source.

The Raman spectrum of Fe/Zn (2:1) exhibits two distinct peaks (Fig. 3c): the D peak centred at 1357 cm^{-1}**,** associated with disordered Turbostratic structures, and the G peak located at 1599 cm^{-1}, attributed to vibrational modes of C=C bonds in graphite crystals. Both peaks correspond to sp^2 bonded carbon atoms (Wang et al. 2003). Similarly, the Raman spectrum of Fe/Zn (1:2) reveals two distinctive peaks:

the wavenumber 1357 cm^{-1} associated with the D peak and the wavenumber 1604 cm^{-1} corresponding to the G peak. The term 'R_I' refers to the ratio of the intensity of the D peak to the intensity of the G peak in the Raman spectrum, providing insight into the degree of well-organized graphite crystallites within carbonaceous materials. A lower R_I value indicates a greater extent of orderly graphitic structure within the nanofibers (Zhou et al. 2009). The R_I value depends on the degree of graphitization and alignment of graphite layers within carbonaceous materials. Generally, a higher position of the G peak in the Raman spectrum (indicating a lower R_I value) corresponds to an increased number of sp^2 graphite bonds within nanofibers, significantly enhancing their structural and mechanical properties (Zhang et al. 2007). In both nanofiber samples, the D peak's intensity exceeds that of the G peak, indicating a greater occurrence of Turbostratic structures over graphitic arrangements.

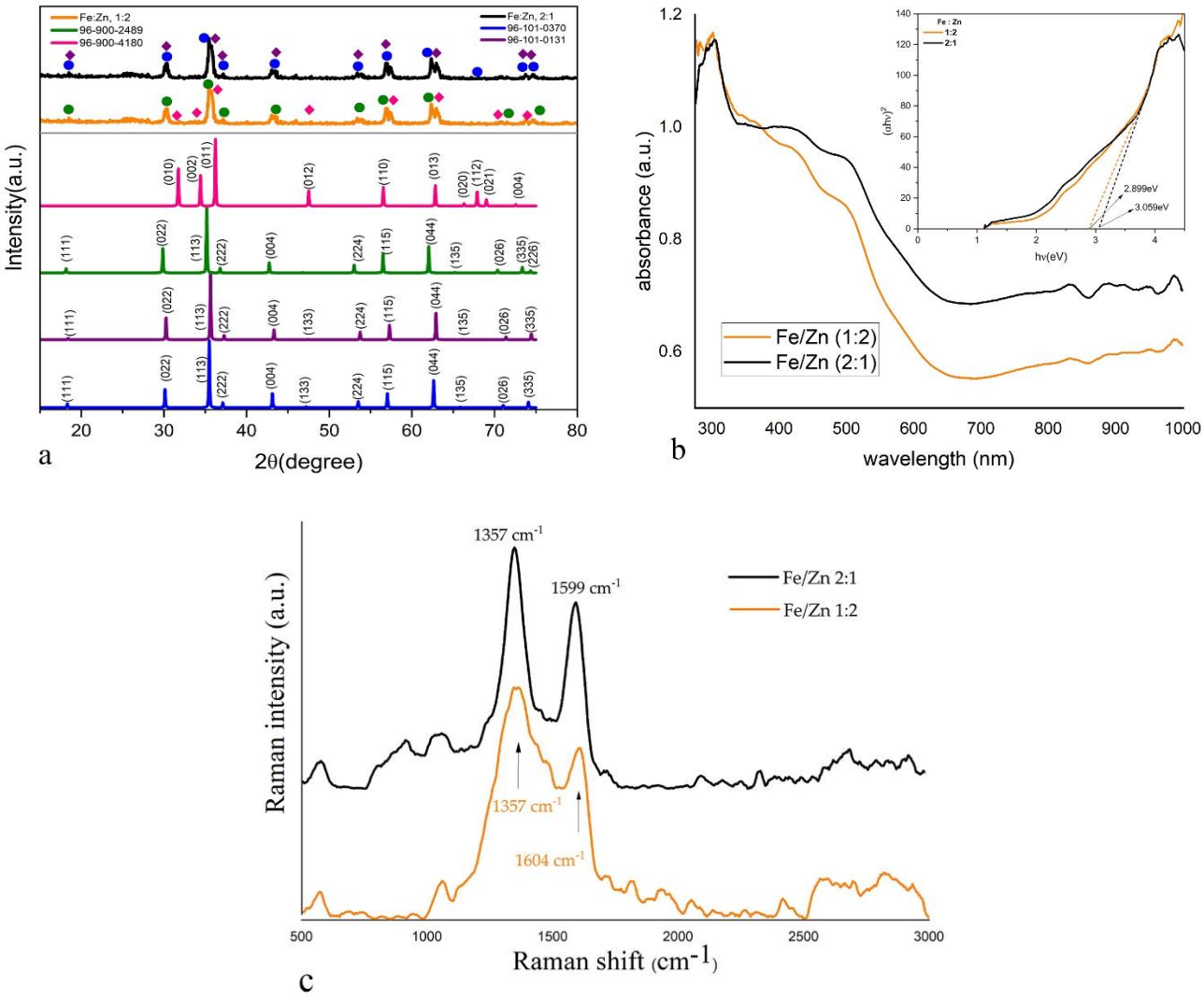

Fig. 3. XRD (a), DRS (b), and Raman spectra (c) of Fe/ZnO nanoparticles-reinforced carbon nanofibers with molar ratios of 1:2 and 2:1.

The nitrogen adsorption isotherms and desorption hysteresis curves for the Fe/Zn (1:2) and Fe/Zn (2:1) samples are shown in Fig. 4. According to the IUPAC classification, the adsorption isotherms of both samples are Type II, and they are accompanied by H2-type and H3-type hysteresis loops for Fe/Zn (1:2)

and Fe/Zn (2:1), respectively. The specific surface areas were measured as 554.18 m²/g and 251.89 m²/g for Fe/Zn (1:2) and Fe/Zn (2:1), respectively, while the respective pore volumes were determined as 0.4866 cm³/g and 0.4733 cm³/g. Further data on the synthesized Fe/Zn (1:2) and Fe/Zn (2:1) samples are presented in Table S3. The significant difference in specific surface area between Fe/Zn (1:2) and Fe/Zn (2:1) can be explained by several factors beyond just the compositional changes: particle size and morphology (Yang et al. 2024), pore structure (Liu et al. 2023), crystal structure and phase composition (Zdainal Abidin et al. 2020), and synergistic effects (Hong et al. 2024).

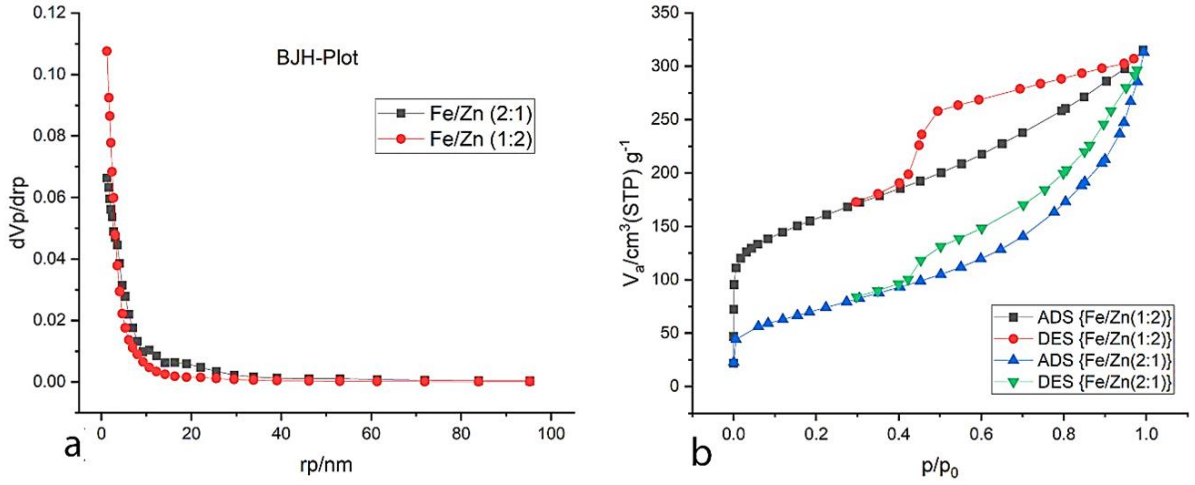

Fig. 4. Nitrogen adsorption-desorption isotherms (a) and corresponding pore size distributions (b) of Fe/ZnO nanoparticles-reinforced carbon nanofibers with molar ratios of 1:2 and 2:1.

The size and solution stability of the nanoparticles were determined by measuring the zeta potential in the range of -400 to +400 mV using a Horiba SZ100 Dynamic Light Scattering (DLS) instrument. The dynamic light scattering and zeta potential measurements of the iron and zinc oxide nanoparticles are presented in Table S3. The average nanoparticle sizes in the Fe/Zn (2:1) and Fe/Zn (1:2) nanofiber samples were approximately 261 nm and 374 nm, respectively. The thermal properties of alloys can influence their nanoparticle size, with iron having higher thermal conductivity than zinc. This difference affects the growth and nucleation of nanoparticles during synthesis, resulting in smaller particle sizes for the Fe/Zn (2:1) alloy (Lamsaf et al. 2022). As shown in Table S4, the zeta potential values for the Fe/Zn (2:1) and Fe/Zn (1:2) nanofibers were -54.4 mV and -46.3 mV, respectively. The significant difference in zeta potential values can be attributed to the particle size, as smaller particles tend to have higher surface charges, resulting in more negative zeta potential values (Rezaei et al. 2023).

3.4. Photocatalytic degradation of Azithromycin

The experimental design consisted of 30 randomized trials, including two center points in each run (Table S5). The response variable representing the photocatalytic degradation percentage of azithromycin was fitted to a linear model and correlated with the independent variables using the

Design-Expert software. The model's adequacy was evaluated using ANOVA (Table S5), which revealed a significant overall model with an F-value of 22.09 and a p-value < 0.0001, indicating a strong correlation between the independent variables and the degradation percentage.

The ANOVA results further showed that all four independent variables pH, reaction time, catalyst dose, and pollutant dose had significant effects on the response, with p-values of <0.0001, 0.0007, 0.0087, and 0.0482, respectively. Among these factors, pH was identified as the most influential variable, with the highest sum of squares (3931.68) and an F-value of 60.46, demonstrating its critical role in azithromycin degradation. The lack-of-fit analysis yielded a p-value of 0.6603, confirming that the model's residuals were well-distributed, and no significant lack-of-fit was observed (Table S6).

To evaluate data normality, a residual plot (Fig. S7a) was analyzed, revealing a predominantly linear trend in the data points, with only two minor exceptions. As noted by Silva et al (2020), the regression model is well-suited for describing the photocatalytic degradation of azithromycin, with the experimental data falling within the residual variance. Homoscedasticity was verified through the residual vs. predicted plot (Fig. S7b), which showed a random dispersion of data points within two red boundary lines. This random distribution indicates constant variance across the data.

Further validation of the model's predictive accuracy is provided by the predicted vs. actual plot (Fig. S7c), where data points are closely aligned along the diagonal, confirming the reliability of the model in predicting degradation percentages. Additionally, a residual vs. run plot (Fig. S7d) was used to assess data trends over time, demonstrating the randomness and independence of residuals from time-dependent factors. The absence of trends in this plot confirms that no latent variables influenced the experimental response, which is supported by Ali et al (2023).

3.4.1. Impact of pH on Azithromycin photocatalytic degradation

The photocatalytic degradation of azithromycin is significantly influenced by the pH of the solution. Generally, the photocatalytic degradation of organic compounds is more efficient under acidic conditions because of several factors.

First, the surface charge of the photocatalyst is modulated by the solution's pH. For instance, Čizmić et al. observed that the surface charge of TiO_2 particles becomes more positive under acidic conditions, facilitating the adsorption of negatively charged azithromycin molecules onto the photocatalyst's surface (Čizmić et al. 2019). Similarly, for Fe/Zn-CNFs, the point of zero charge (PZC) is a critical parameter; below the PZC, the positively charged surface enhances the interaction with negatively charged azithromycin molecules, promoting photocatalytic activity.

Second, acidic conditions enhance the generation of hydroxyl radicals (•OH), which are highly reactive species capable of degrading azithromycin (Rodríguez-López et al. 2022). During the photocatalytic degradation cycle, electrons from the photocatalyst are transferred to oxygen molecules, producing superoxide radicals ($\bullet O_2^-$). In an acidic environment, these radicals react with hydrogen ions (H^+) to form hydroperoxyl radicals ($\bullet HO_2$), which subsequently undergo homolytic cleavage to generate

hydroxyl radicals (•OH). These hydroxyl radicals attack on azithromycin molecules, ultimately leading to their degradation (Rodríguez-López et al. 2022).

In addition, acidic conditions enhance the solubility of azithromycin, thereby increasing its ability to be degradation by the photocatalyst. This combination of increased solubility, production of reactive oxygen species, and pH-mediated changes in the photocatalyst's surface charge contributes to the higher efficiency of azithromycin degradation under acidic conditions (Sayadi et al. 2019). Quantitative results support these findings. At pH 3, the degradation efficiency of azithromycin reached 97.5%, compared to 88.2% at pH 7 and 74.6% at pH 10 under optimal reaction conditions. This underscores the significant role of pH in optimizing the photocatalytic performance. Among the variables studied, pH demonstrated the most substantial impact on azithromycin degradation, with an observed 1.10-fold increase in efficiency at acidic pH compared to neutral pH. The statistical significance of pH as a factor was validated through ANOVA (Table S5), where p-values < 0.0001 confirmed its strong influence on the degradation process. Additionally, the three-dimensional response surface plot (Fig. 5a) illustrates the effect of pH on azithromycin degradation, further highlighting the enhanced efficiency in acidic environments.

3.4.2. Impact of catalyst concentration on the photocatalytic degradation of Azithromycin

As shown in Fig. 5b, the photocatalytic degradation efficiency of azithromycin increases with increasing Fe/Zn-CNF loading, peaking at 30 mg/L under pH 4. This enhancement can be attributed to the increased surface area, which provides a greater number of active sites, and more favourable interactions between azithromycin and the catalyst. At this optimal concentration, the catalyst is fully utilized without the saturation of active sites.

However, increasing the nanocatalyst concentration beyond this point does not further improve the removal efficiency. In fact, excess catalyst loading can result in the aggregation of nanoparticles, leading to increased turbidity. This aggregation obstructs light penetration, which is crucial for photocatalytic activity, thus reducing the overall efficiency (Yazdani and Sayadi 2018; Al-Nuaim et al. 2023). Therefore, it is essential to carefully balance the catalyst concentration to optimize the photocatalytic performance. This insight is particularly important for large-scale applications, where efficiency and cost-effectiveness must be balanced.

3.4.3. Impact of Azithromycin concentration on photocatalytic degradation

Numerous studies have indicated a decline in the photocatalytic activity of catalysts at higher initial pollutant concentrations, with improved degradation efficiency observed at lower concentrations (Chen et al. 2018). This behavior is attributed to the saturation of surface-active sites on the photocatalyst at elevated pollutant concentrations, leading to a decrease in photocatalytic efficiency. As shown in Figure 5c, the photocatalytic degradation of azithromycin decreases with increasing concentration, indicating that azithromycin molecules occupy the active sites of the catalyst, leaving fewer sites available for

adsorption. While •OH radicals are still generated in constant amounts, their interaction with the pollutants becomes less efficient as the number of available active sites diminish. This reduction in efficiency can be attributed to the competition for •OH radicals, which are also consumed by intermediary compounds generated during the degradation process (Chamanehpour et al. 2023).

Supporting this, Ruziwa et al. found that at higher pollutant concentrations, more •OH radicals are required to effectively degrade pollutants (Ruziwa et al. 2023). However, as more intermediates form, they compete for the available •OH, reducing its availability for the degradation of azithromycin. This indicates that, although higher concentrations of azithromycin require more catalyst loading or longer reaction times for effective degradation, there is an optimal concentration range in which the photocatalytic efficiency is maximized. This finding is consistent with those of previous studies (Shokri et al. 2019; Guo et al. 2020; Lupu et al. 2023) that highlighted the importance of balancing pollutant concentration with catalyst efficiency.

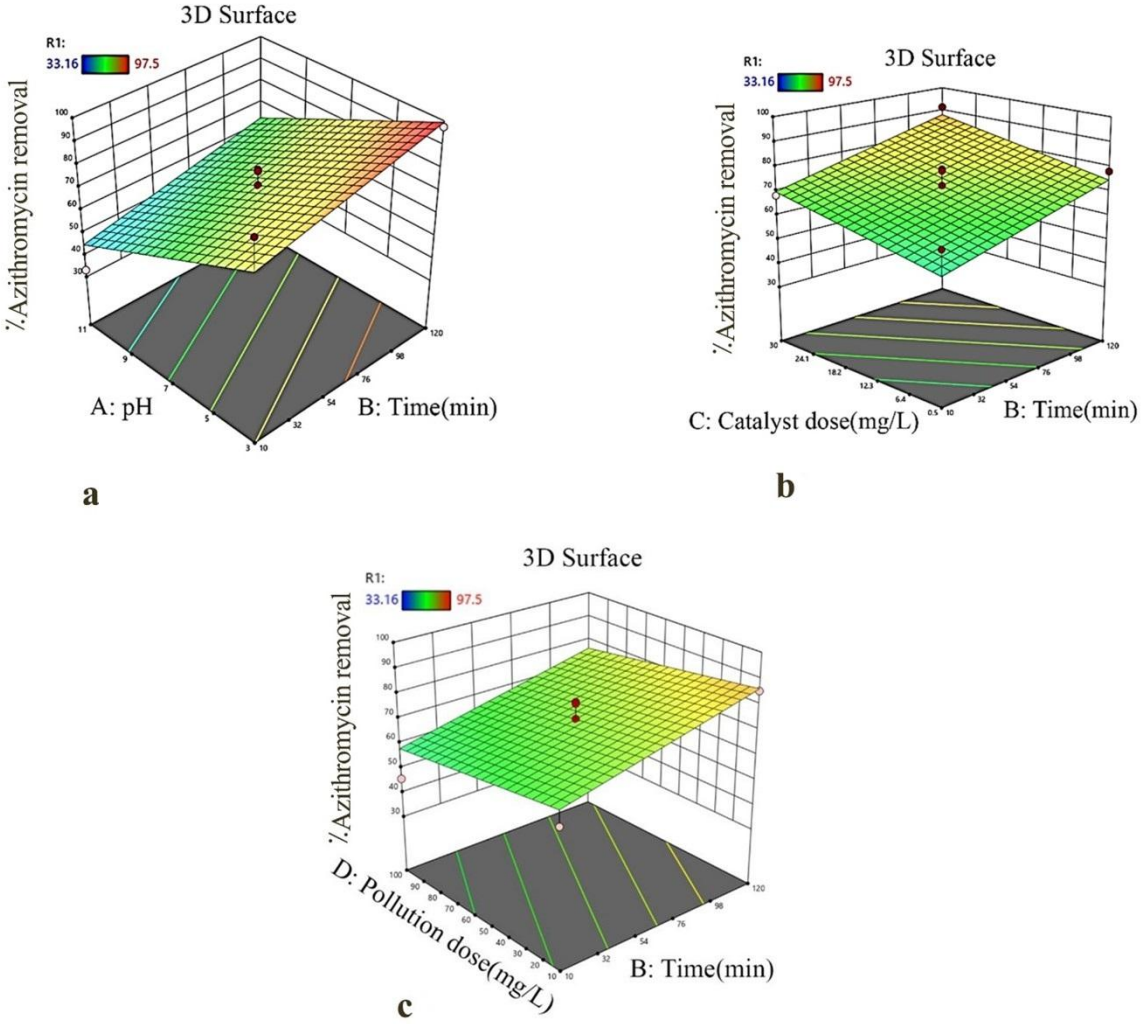

Fig. 5. The effect of pH (a), catalyst dose (b), and pollution dose (c) on the photocatalytic degradation of azithromycin under optimal conditions

3.4.4. Impact of reaction time on Azithromycin photocatalytic degradation

The duration of irradiation is a critical parameter in the photocatalytic degradation of pollutants because it directly affects the efficiency of the degradation process (Molla et al. 2020). As shown in Figure 5c, the photocatalytic degradation efficiency of azithromycin increases significantly as the irradiation time is extended from 10 to 120 min. Specifically, after 60 min, the degradation efficiency exceeds 82.4% and continues to improve, reaching 97.1% after 120 min. This trend demonstrates the importance of sufficient exposure time to achieve maximum pollutant breakdown. This enhancement can be primarily attributed to the prolonged availability of active sites on the photocatalyst surface, which allows for sustained interactions between the catalyst and azithromycin molecules. Additionally, the generation of hydroxyl radicals (•OH), which are essential for the degradation process, was more pronounced with an extended irradiation time. The longer reaction period provides sufficient time for these hydroxyl radicals to form and interact with the azithromycin molecules, resulting in the breakdown of the antibiotic (Kalantar et al. 2023; Bazrafshan et al. 2023). Over time, the continuous production of hydroxyl radicals ensures that more active sites on the catalyst are engaged, and the reactive species have enough time to effectively degrade the organic pollutants.

3.4.5. Optimization of the photocatalytic degradation of Azithromycin

The optimal reaction conditions for the photocatalytic degradation of azithromycin were determined by analysis of the Box-Behnken Design (BBD) model. The conditions that resulted in the highest degradation efficiency are summarized in Table 1. The optimal values identified were a reaction time of 103 min, catalyst concentration of 27.1 mg/L, pH of 4, and azithromycin concentration of 15.8 mg/L. To validate the accuracy of the model predictions, two experimental tests were conducted under optimal conditions. The experimental degradation value of azithromycin in the Fe/Zn (2:1) sample was 98.1%, which closely aligned with the model predicted value. Similarly, in the Fe/Zn (1:2) sample, 93.9% of azithromycin was degraded under these conditions, further confirming the model's reliability in predicting the degradation process.

Table 1. Optimal conditions for AZM degradation according to BBD model

Sample	pH	Time (min)	Catalyst dose (mg/L)	Pollution dose (mg/L)	Removal (%)	Desirability
Fe/ZnO (2:1)	4	103	27.1	15.8	98.1	1.0
Fe/ZnO (1:2)					93.9	

The effectiveness of the photocatalytic degradation of azithromycin under optimal conditions has been confirmed by other studies. For instance, Sharma et al. (2023) reported promising results for treating wastewater containing azithromycin under similar ideal conditions. In their study, photocatalytic degradation was achieved after 90 min of treatment, using Cu_2O-TiO_2 nanotubes at a concentration of 1.5 g/L and azithromycin at a concentration of 100 μg/mL at neutral pH. In another investigation,

Mehrdoost et al. (2022). utilized the PAC/Fe/Ag/Zn nanocomposite to degrade azithromycin, with efficiencies ranging from 40% to 99.5% over four consecutive cycles and 120 min of reaction time. These results highlight the effectiveness of the optimized conditions for enhancing the photocatalytic degradation of azithromycin and highlight the potential for scaling up this process in wastewater treatment applications.

3.4.6. Effect of light source on the photocatalytic degradation efficiency of Azithromycin

To evaluate the impact of different light sources on the degradation efficiency of azithromycin, experiments were conducted under UV, visible, and dark conditions. The initial azithromycin concentration was set at 15.8 mg/L, with a catalyst loading of 27.1 mg/L, and an initial pH of 4 (optimal conditions). Fig. 6 illustrates the degradation efficiency of azithromycin under these conditions.

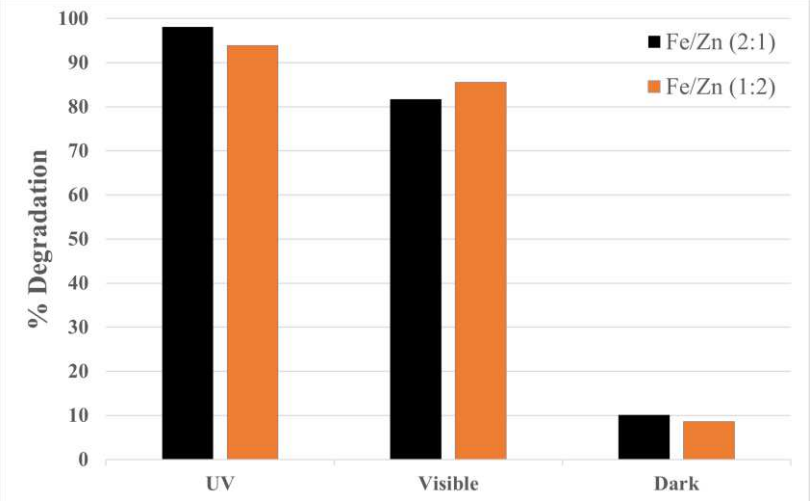

Fig. 6. Percentage of photocatalytic degradation of azithromycin under various light sources and optimal conditions

The Fe/Zn (2:1) and Fe/Zn (1:2) catalysts demonstrated nearly complete degradation under UV light, achieving approximately 98% degradation within 103 min. Under visible light, significant degradation was observed, reaching 85% for Fe/Zn (2:1) and 81% for Fe/Zn (1:2). This relatively high efficiency under visible light can be attributed to the Fe-doping of ZnO, which enhances the photocatalytic activity by narrowing the bandgap and improving light absorption in the visible range. The remarkable photocatalytic performance of Fe/Zn-CNFs under both UV and visible light is linked to their reduced bandgap energy. As shown in the absorption spectrum of Fe/Zn-CNFs in Figure 3b, this material exhibits significant absorption in the wavelength range of 300–500 nm, enabling effective absorption of both UV and visible light.

To clarify the role of active species in the photocatalytic degradation of azithromycin, a crucial preliminary step was performed to ensure effective adsorption of the antibiotic onto the catalyst surface. The catalyst-azithromycin mixture was maintained in darkness for 30 min to establish adsorption-

desorption equilibrium before light exposure. This controlled equilibration step is vital for isolating the adsorption process from photochemical reactions, preventing interference from light-induced catalytic activity (Yu et al. 2019). Quenching experiments conducted in this context provided significant insights into the roles of active species in the degradation process under UV, visible, and reactive species, such as hydroxyl radicals (•OH), superoxide radicals ($•O^{2-}$), and holes (h^+). These findings identified the primary active species responsible for the degradation of azithromycin. By ensuring these conditions, the present study offers a robust foundation for understanding the catalyst performance and clarifying its degradation mechanism.

3.5. The mechanism and kinetics of photocatalytic degradation of Azithromycin

Photocatalysts accelerate chemical reactions when exposed to light, a phenomenon known as photocatalysis. This process involves the use of light in conjunction with a semiconductor substrate. A material that absorbs light and facilitates the catalysis of chemical reactions is referred to as a photocatalyst, and it typically consists of a semiconductor. In photocatalysis, the exposure of a semiconducting material to light generates an electron-hole pair (Ameta et al. 2018). Fig. 7 illustrates the photocatalytic degradation mechanism of azithromycin using the Fe/Zn-CNFs catalyst.

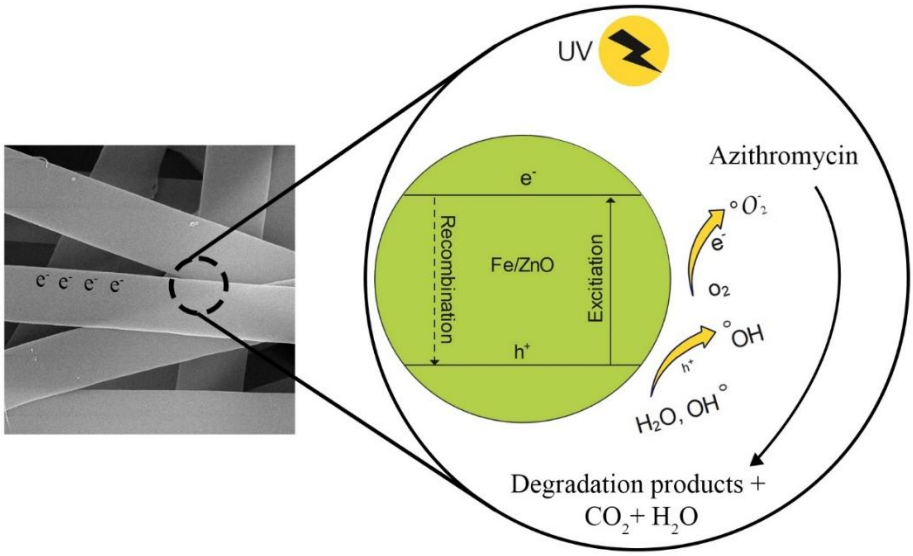

Fig. 7. Schematic diagram of the photocatalytic degradation of azithromycin by Fe/Zn-CNFs.

Reactions (5-12) illustrate the generation of •OH via the following photocatalytic process:

$$Fe/Zn - CNFs + hv \rightarrow Fe/Zn - CNFs\ (e^- + h^+) \quad (5)$$

$$h^+ + H_2O \rightarrow h^+ + \bullet OH \quad (6)$$

$$h^+ + OH^- \rightarrow \bullet OH \quad (7)$$

$$Fe^{3+} + e^- \rightarrow Fe^{2+} \quad (8)$$

$$e^- + O_2 \rightarrow \bullet O_2^- \quad (9)$$

$$\bullet O_2^- + H_2O + h^+ \rightarrow H_2O_2 + OH^- \quad (10)$$

$$H_2O_2 + e^- \rightarrow \bullet OH + OH^- \quad (11)$$

$$Azithromycin\ Antibiotic + \bullet OH \rightarrow Degradation\ Products \quad (12)$$

During the photocatalytic degradation of azithromycin, various intermediates are formed through distinct chemical modifications of the original compound (Tong et al. 2011; Luo et al. 2016; Kadmi et al. 2025). A notable intermediate is desosaminyl lazithromycin ($C_{10}H_9NO$), which has been confirmed to be the main degradation product of this photocatalytic process. Other intermediates include hydroxylation-dehydration products ($C_6H_{12}O_3N$), which result from the addition of hydroxyl groups to the azithromycin structure, and methylation products ($C_5H_{10}NO$), which are generated through methylation reactions that further modify the antibiotic.

These transformations occur as hydroxyl radicals ($^{\bullet}OH$) actively attack the amino sugar and cladinose components of azithromycin, initiating a complex series of reactions (Tong et al. 2011; Luo et al. 2016; Kadmi et al. 2025). The degradation process may also yield smaller organic fragments, such as C_5H_7O, which could include various ketones or aldehydes. This intricate network of reactions highlights the importance of understanding the intermediates formed during degradation, as they can provide insights into the degradation mechanism and inform evaluations of the potential toxicity and environmental impact of the by-products produced in the treatment of azithromycin and similar pharmaceutical contaminants.

Under optimal conditions pH 4, catalyst concentration of Fe/Zn-CNFs at 27.1 mg/L, an azithromycin concentration of 15.8 mg/L, and a reaction time of 103min the studies on azithromycin photocatalytic degradation kinetics reveal that the reaction follows first-order kinetics. This result is further supported by the linear degradation reaction curves shown in Fig. 8, which illustrate the efficient and predictable nature of the degradation process facilitated by the photocatalysts.

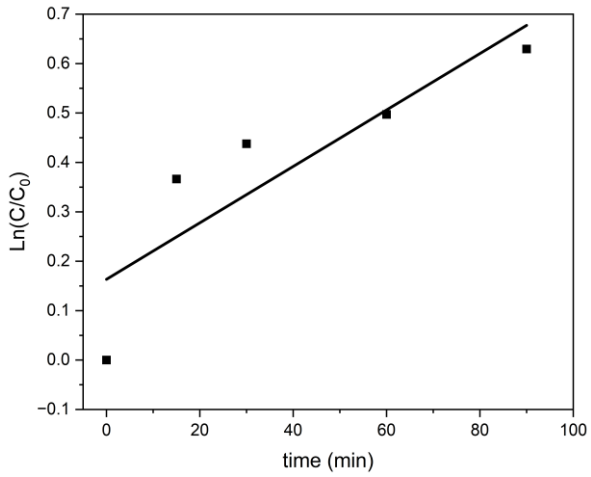

Fig. 8. Kinetics of azithromycin photocatalytic degradation using Fe/Zn nanoparticle-reinforced carbon nanofibers

3.6. Stability and reusability of Fe/Zn-CNFs for photocatalytic Azithromycin degradation

The stability and reusability of photocatalysts are key parameters that determine their practicality in large-scale wastewater treatment applications. The study tested Fe/Zn-reinforced carbon nanofibers for the degradation of azithromycin over five reuse cycles under optimal conditions. The photocatalytic performance was evaluated by measuring the concentration of residual azithromycin at the end of each cycle. The results demonstrate (Fig. 9) that the Fe/Zn-CNFs maintained a high degradation efficiency over five cycles, with the degradation efficiency exceeding 80% in the final cycle. A slight reduction in efficiency was observed, which is likely due to partial contamination, minor agglomeration, or gradual deactivation of the photocatalyst over repeated cycles. The durability and reusability of Fe/Zn-CNFs are attributed to their durable structural integrity, efficient magnetic recovery, and synergistic interactions between the Fe/Zn oxide nanoparticles and the carbon nanofiber matrix, which collectively enhance their photocatalytic activity and longevity. These findings highlight the potential of Fe/Zn-CNFs as reliable, sustainable, and cost-effective photocatalysts for pharmaceutical wastewater treatment. By retaining significant degradation efficiency even after multiple cycles, Fe/Zn-CNFs demonstrate the feasibility of their application in real-world scenarios, thus addressing the need for recyclable materials in environmental remediation technologies.

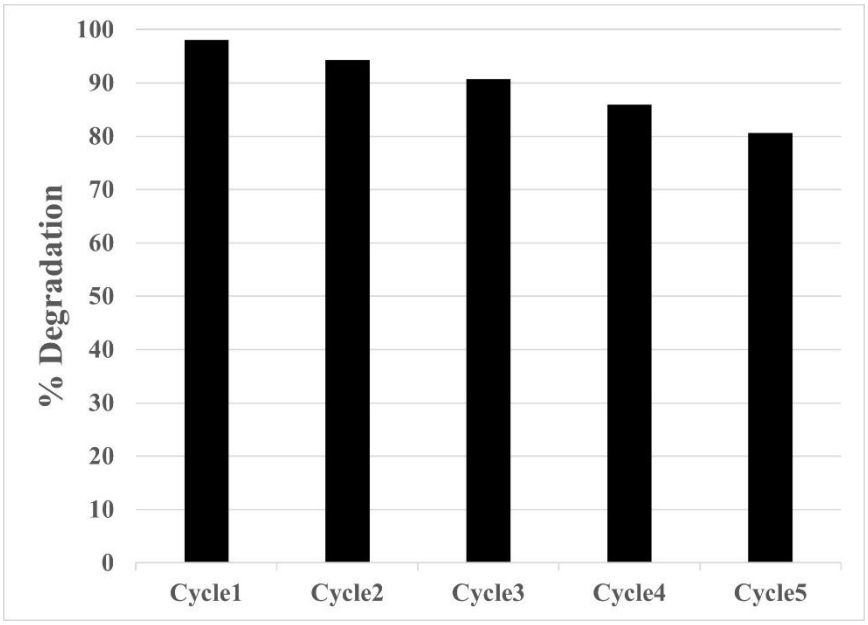

Fig. 9. Reusability of Fe/Zn-CNFs for photocatalytic degradation of azithromycin under optimal conditions over five cycles

3.7. Antibacterial performance of Fe/Zn-CNFs

Metallic elements and metal oxides have potent antibacterial activities for treating various bacterial diseases. Among these, zinc oxide nanoparticles (ZnO-NPs) have received considerable attention globally owing to their natural antibacterial properties (Sirelkhatim et al. 2015). The Fe/Zn nanofibers formulated in different molar ratios exhibit varying inhibition zones against both Gram-positive and Gram-negative bacteria (Fig. 10). Although the exact mechanism of the effects of ZnO-NPs is not fully understood, studies have suggested their ability to inhibit the growth of diverse bacterial strains (Mendes et al. 2022a). As shown in Table 2, Fe/Zn (1:2) nanofibers exhibit inhibition zones of 22.5 ± 1.3 mm against *S. aureus* and 18.7 ± 1.2 mm against *E. coli*, whereas Fe/Zn (2:1) nanofibers exhibit inhibition zones of 21.3 ± 1.2 mm against *S. aureus* and 15.5 ± 1.3 mm against *E. coli*. These variations in inhibition zones can be attributed to differences in bacterial sensitivity and the specific properties of the nanoparticles.

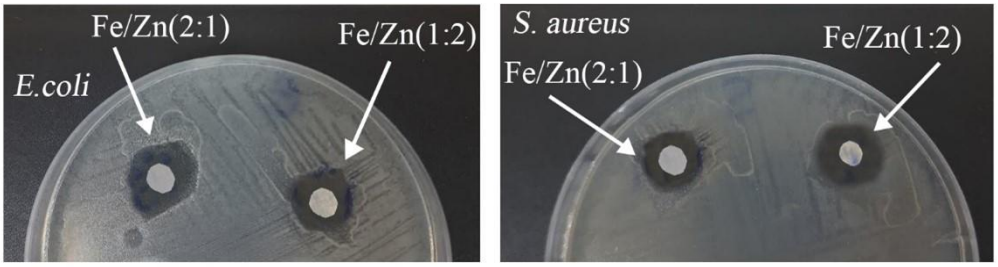

Fig. 10. Antibacterial activity of Fe/Zn nanofibers against *S. aureus* and *E. coli*

Table 2. Average inhibition zones of antibacterial activity for Fe/Zn nanofibers, measured in triplicate against two distinct bacterial strains

Bacterial Strains	Fe/Zn (1:2)	Fe/Zn (2:1)
S. aureus	22.5±1.3	21.3±1.2
E. coli	18.7±1.2	15.5±1.3

The antibacterial action of ZnO-NPs is primarily attributed to their production of reactive oxygen species (ROS), which impede bacterial growth through several mechanisms. Upon contact with bacteria, ZnO-NPs generate ROS, including hydrogen peroxide and superoxide radicals. These ROS can induce oxidative stress and damage bacterial cells. Furthermore, increased ROS levels can lead to lipid peroxidation of the bacterial cell membrane, disrupting its integrity and functionality. This disruption can destabilize the membrane, causing leakage of cellular contents, loss of essential functions, and ultimately leading to bacterial death (Tiwari et al. 2018).

Findings from this study, along with recent research, indicate that the antibacterial efficacy of ZnO-NPs is more pronounced against *S. aureus* than against *E. coli*. It is important to note that the antibacterial property assessments were conducted in triplicate, and the averages shown in Table 2 reflect these

measurements. The generation of ROS by ZnO-NPs is a critical mechanism underlying their antibacterial activity**.** Studies have demonstrated that ROS production by ZnO-NPs is more effective against *S. aureus* than *E. coli* (Jones et al. 2008; Lallo da Silva et al. 2019; Mendes et al. 2022b).

4. Conclusion

This study demonstrated the potential of iron/zinc oxide nanoparticle-reinforced carbon nanofibers, synthesized via electrospinning, for photocatalytic degradation of the azithromycin in aqueous solutions. The experimental analysis confirmed that the iron/zinc oxide nanoparticles were successfully incorporated into the carbon nanofiber matrix, as verified by XRD, Raman, and DRS analyses, which demonstrated the crystalline structure and optimal bandgap energy of the nanofibers. The Fe/Zn (1:2) catalyst exhibited a narrower bandgap (2.899 eV) compared to pure ZnO (3.37 eV), enabling enhanced photocatalytic activity under UV light and achieving a degradation efficiency of over 97.5% of azithromycin under optimal conditions. Furthermore, the Response Surface Methodology (RSM) optimization identified the highest degradation efficiency at a reaction time of 103 min, with a catalyst dose of 27.1 mg/L, pH 4, and azithromycin concentration of 15.8 mg/L, which corresponds to the catalyst's optimized bandgap. The effect of the light source was also investigated, demonstrating that Fe/Zn-CNFs exhibit remarkable degradation efficiency under both UV and visible light. Specifically, the Fe/Zn (2:1) and Fe/Zn (1:2) catalysts achieved nearly complete degradation of azithromycin (approximately 98%) under UV light, while under visible light, the degradation efficiency reached 85% and 81%, respectively. The ability to use visible light further underscores the versatility of Fe/Zn-CNFs as photocatalysts. The stability and reusability of the Fe/Zn-CNFs were evaluated over five consecutive cycles under optimal conditions. The results indicate that the photocatalyst maintained over 80% degradation efficiency in the final cycle, highlighting its excellent reusability and stability. This stability is critical for practical applications in wastewater treatment. The superior photocatalytic performance can be attributed to the synergetic interaction between the iron and zinc oxide nanoparticles and the carbon nanofiber matrix, which enhanced the surface area, increased the number of reactive sites, and promoted efficient charge separation. Additionally, the nanofibers exhibited antibacterial efficacy against *E. coli* and *S. aureus*, likely due to the generation of reactive oxygen species, which inhibit the proliferation of antibiotic-resistant bacteria. In conclusion, iron/zinc oxide nanoparticle-reinforced carbon nanofibers demonstrated excellent photocatalytic degradation efficiency, stability, reusability, and antibacterial properties, highlighting their potential as an effective solution for pharmaceutical wastewater treatment. These findings mark a significant advancement in the utilization of nanotechnology to degrade of antibiotic pollutants and reduce antibiotic resistance in water systems.

Declarations

-Ethical Approval

Not applicable.

-Consent to Participate

Not applicable.

-Consent to Publish

Not applicable.

-Authors Contributions

CRediT authorship contribution statement **Poorya Hosseinabadi**: Conceptualization, Data curation, Formal analysis, Investigation, Methodology, Validation, Visualization, Writing – original draft, and Writing – review & editing. **Mohammad Reza Rezaei**: Conceptualization, Investigation, Validation, Methodology, and Supervision. **Mohammad Hossein Sayadi**: Methodology, and Supervision. **Hossein Barani**: Funding acquisition, Methodology, Project administration, Supervision, and Writing – review & editing.

-Funding

No Funding

-Competing Interests

The authors declare no competing interests.

-Availability of data and materials

The data and materials used in this study are available from the corresponding author upon reasonable request.

References:

Al-Hakkani MF, Gouda GA, Hassan SHA, Mohamed MMA, Nagiub AM (2022) Environmentally azithromycin pharmaceutical wastewater management and synergetic biocompatible approaches of loaded azithromycin@hematite nanoparticles. Sci Rep 12:10970. https://doi.org/10.1038/s41598-022-14997-y

Al-Nuaim MA, Alwasiti AA, Shnain ZY (2023) The photocatalytic process in the treatment of polluted water. Chem zvesti 77:677–701. https://doi.org/10.1007/s11696-022-02468-7

Alam U, Khan A, Ali D, Bahnemann D, Muneer M (2018) Comparative photocatalytic activity of sol–gel derived rare earth metal (La, Nd, Sm and Dy)-doped ZnO photocatalysts for degradation of dyes. RSC Adv 8:17582–17594. https://doi.org/10.1039/C8RA01638K

Alharshan GA, Aboraia AM, Uosif MAM, Sharaf IM, Shaaban ER, Saad M, ALMohiy H, Elsenety MM (2023) Optical Band Gap Tuning, DFT Understandings, and Photocatalysis Performance of ZnO Nanoparticle-Doped Fe Compounds. Mater (Basel, Switzerland) 16:. https://doi.org/10.3390/ma16072676

Ali H, Yasir M, Ngwabebhoh FA, Sopik T, Zandraa O, Sevcik J, Masar M, Machovsky M, Kuritka I (2023) Boosting photocatalytic degradation of estrone hormone by silica-supported g-C3N4/WO3 using response surface methodology coupled with Box-Behnken design. J

Photochem Photobiol A Chem 441:114733. https://doi.org/https://doi.org/10.1016/j.jphotochem.2023.114733

Ameta R, Solanki MS, Benjamin S, Ameta SC (2018) Photocatalysis. In: Advanced oxidation processes for waste water treatment. Elsevier, pp 135–175

Bakina O, Glazkova E, Rodkevich N, Mosunov A, Chzhou V, Lerner M (2022) Electroexplosive synthesis of composite ZnO/ZnFe2O4/Zn nanoparticles with photocatalytic and antibacterial activity. Mater Sci Semicond Process 152:107076. https://doi.org/https://doi.org/10.1016/j.mssp.2022.107076

Barani H, Khorashadizadeh M, Haseloer A, Klein A (2020) Characterization and Release Behavior of a Thiosemicarbazone from Electrospun Polyvinyl Alcohol Core-Shell Nanofibers. Polymers (Basel). 12

Bazrafshan E, Mohammadi L, Zarei AA, Mosafer J, Zafar MN, Dargahi A (2023) Optimization of the photocatalytic degradation of phenol using superparamagnetic iron oxide (Fe(3)O(4)) nanoparticles in aqueous solutions. RSC Adv 13:25408–25424. https://doi.org/10.1039/d3ra03612j

Chamanehpour E, Hossein Sayadi M, Hajiani M (2023) Metal-organic framework coordinated with g-C3N4 and metal ions for boosting photocatalytic H2 production under sunlight. J Photochem Photobiol A Chem 434:114221. https://doi.org/https://doi.org/10.1016/j.jphotochem.2022.114221

Chavoshan S, Khodadadi M, Nasseh N (2020) Photocatalytic degradation of penicillin G from simulated wastewater using the UV/ZnO process: isotherm and kinetic study. J Environ Heal Sci Eng 18:107–117. https://doi.org/10.1007/s40201-020-00442-7

Chen F, Li S, Chen Q, Zheng X, Liu P, Fang S (2018) 3D graphene aerogels-supported Ag and Ag@ Ag3PO4 heterostructure for the efficient adsorption-photocatalysis capture of different dye pollutants in water. Mater Res Bull 105:334–341

Chen X, Wu Z, Liu D, Gao Z (2017) Preparation of ZnO Photocatalyst for the Efficient and Rapid Photocatalytic Degradation of Azo Dyes. Nanoscale Res Lett 12:143. https://doi.org/10.1186/s11671-017-1904-4

Čizmić M, Ljubas D, Rožman M, Ašperger D, Ćurković L, Babić S (2019) Photocatalytic Degradation of Azithromycin by Nanostructured TiO_2 Film: Kinetics, Degradation Products, and Toxicity. Mater (Basel, Switzerland) 12:. https://doi.org/10.3390/ma12060873

Dharmana G, Gurugubelli TR, Viswanadham B, Bathula B, Yoo K (2023) Novel In Situ Fabrication of Fe-Doped Zinc Oxide/Tin Sulfide Heterostructures for Visible-Light-Driven Photocatalytic Degradation of Methylene Blue. J Chem 2023:1407395

Fiszka Borzyszkowska A, Sulowska A, Zekker I, Karczewski J, Bester K, Zielińska-Jurek A (2022) Environmentally Friendly Fabrication of High-Efficient Fe-ZnO/Citric Acid-Modified Cellulose Composite and the Enhancement of Photocatalytic Activity in the Presence of H2O2. Catalysts

12

Godin R, Hisatomi T, Domen K, Durrant JR (2018) Understanding the visible-light photocatalytic activity of GaN: ZnO solid solution: the role of Rh 2− y Cr y O 3 cocatalyst and charge carrier lifetimes over tens of seconds. Chem Sci 9:7546–7555

Golrizkhatami F, Taghavi L, Nasseh N, Panahi HA (2023) Synthesis of novel MnFe2O4/BiOI green nanocomposite and its application to photocatalytic degradation of tetracycline hydrochloride: (LC-MS analyses, mechanism, reusability, kinetic, radical agents, mineralization, process capability, and purification of . J Photochem Photobiol A Chem 444:114989. https://doi.org/https://doi.org/10.1016/j.jphotochem.2023.114989

Guo K, Zheng S, Zhang X, Zhao L, Ji S, Chen C, Wu Z, Wang D, Fang J (2020) Roles of bromine radicals and hydroxyl radicals in the degradation of micropollutants by the UV/bromine process. Environ Sci Technol 54:6415–6426

Hong G, Shan R, Gu J, Huhe T, Yuan H, Chen Y (2024) Fe-Zn bimetallic oxide functionalized biochar for enhanced adsorption of enrofloxacin in water. J Environ Chem Eng 12:112208. https://doi.org/https://doi.org/10.1016/j.jece.2024.112208

Hu L, Dong S, Li Q, Feng J, Pi Y, Liu M, Sun J, Sun J (2015) Facile synthesis of BiOF/Bi2O3/reduced graphene oxide photocatalyst with highly efficient and stable natural sunlight photocatalytic performance. J Alloys Compd 633:256–264

Jayanna BK, Nagendrappa G, Arunkumar, Gowda N (2012) Spectrophotometric estimation of azithromycin in tablets. Indian J Pharm Sci 74:365–367. https://doi.org/10.4103/0250-474X.107076

Jones N, Ray B, Ranjit KT, Manna AC (2008) Antibacterial activity of ZnO nanoparticle suspensions on a broad spectrum of microorganisms. FEMS Microbiol Lett 279:71–76. https://doi.org/https://doi.org/10.1111/j.1574-6968.2007.01012.x

Kadmi Y, Ousaadi MI, Lakhdari D, Bachiri N, Bouta I, Bouizzar S, Joo S-W, Vasseghian Y, Lakhdari N, Berkani M (2025) Optimization of azithromycin degradation: Integrating ANN-PSO modeling, intermediates analysis, identification, and microbiological assessment. J Taiwan Inst Chem Eng 166:105086

Kalantar S, Bemani A, Sayadi MH, Chamanehpour E (2023) Visible light–driven ZnO/Fe3O4 magnetic nanoparticles for detoxification of diazinon: the photocatalytic optimization process with RSM-BBD model. Environ Sci Pollut Res 30:95634–95647. https://doi.org/10.1007/s11356-023-29024-4

Karimi L, Zohoori S, Yazdanshenas ME (2014) Photocatalytic degradation of azo dyes in aqueous solutions under UV irradiation using nano-strontium titanate as the nanophotocatalyst. J Saudi Chem Soc 18:581–588. https://doi.org/https://doi.org/10.1016/j.jscs.2011.11.010

Kaswan V, Kaur H (2023) A comparative study of advanced oxidation processes for wastewater treatment. Water Pract Technol 18:1233–1254. https://doi.org/10.2166/wpt.2023.061

Kayaci F, Vempati S, Donmez I, Biyikli N, Uyar T (2014) Role of zinc interstitials and oxygen vacancies of ZnO in photocatalysis: a bottom-up approach to control defect density. Nanoscale 6:10224–10234. https://doi.org/10.1039/C4NR01887G

Khan P, Saha R, Halder G (2024) Towards sorptive eradication of pharmaceutical micro-pollutant ciprofloxacin from aquatic environment: A comprehensive review. Sci Total Environ 919:170723. https://doi.org/https://doi.org/10.1016/j.scitotenv.2024.170723

Lallo da Silva B, Caetano BL, Chiari-Andréo BG, Pietro RCLR, Chiavacci LA (2019) Increased antibacterial activity of ZnO nanoparticles: Influence of size and surface modification. Colloids Surfaces B Biointerfaces 177:440–447. https://doi.org/https://doi.org/10.1016/j.colsurfb.2019.02.013

Lambora S, Bhardwaj A (2023) Morphology Transition with Temperature and its Effect on Optical Properties of Colloidal MoS(2) Nanostructures. ACS omega 8:27725–27731. https://doi.org/10.1021/acsomega.3c03478

Lamsaf H, Ballesteros LF, Cerqueira MA, Teixeira JA, Pastrana LM, Rebouta L, Carvalho S, Calderon S (2022) Zn and Zn-Fe Nanostructures with Multifunctional Properties as Components for Food Packaging Materials. Nanomater (Basel, Switzerland) 12:. https://doi.org/10.3390/nano12122104

Lin L, Jiang W, Nasr M, Bechelany M, Miele P, Wang H, Xu P (2019) Enhanced visible light photocatalysis by TiO2–BN enabled electrospinning of nanofibers for pharmaceutical degradation and wastewater treatment. Photochem Photobiol Sci 18:2921–2930. https://doi.org/10.1039/c9pp00304e

Liu Y, Ji X, Wang Y, Zhang Y, Zhang Y, Li W, Yuan J, Ma D, Sun H, Duan J (2023) A Stable Fe-Zn Modified Sludge-Derived Biochar for Diuron Removal: Kinetics, Isotherms, Mechanism, and Practical Research. Molecules 28

Luo X, Hao T, Yue L, Hong G, Lu Y (2016) Azithromycin wastewater treatment with la doping titanium dioxide/active carbon composites. In: 2015 4th International Conference on Sensors, Measurement and Intelligent Materials. Atlantis Press, pp 861–870

Lupu G-I, Orbeci C, Bobirică C, Bobirică L, Lazăr ES, Pandele-Cusu J, Verziu MN, Pîrvu C, Irodia R-G (2023) Photocatalytic degradation of azithromycin formulation in aqueous solution by doped titanium dioxide/fiberglass-rubberized silicone photocatalytic membrane. Sustain Environ Res 33:36

Marinho BA, Suhadolnik L, Likozar B, Huš M, Marinko Ž, Čeh M (2022) Photocatalytic, electrocatalytic and photoelectrocatalytic degradation of pharmaceuticals in aqueous media: Analytical methods, mechanisms, simulations, catalysts and reactors. J Clean Prod 131061

Mehrdoost A, Yengejeh RJ, Mohammadi MK, Haghighatzadeh A, Babaei AA (2022) Adsorption removal and photocatalytic degradation of azithromycin from aqueous solution using PAC/Fe/Ag/Zn nanocomposite. Environ Sci Pollut Res 29:33514–33527.

https://doi.org/10.1007/s11356-021-18158-y

Mendes CR, Dilarri G, Forsan CF, Sapata V de MR, Lopes PRM, de Moraes PB, Montagnolli RN, Ferreira H, Bidoia ED (2022a) Antibacterial action and target mechanisms of zinc oxide nanoparticles against bacterial pathogens. Sci Rep 12:2658. https://doi.org/10.1038/s41598-022-06657-y

Mendes CR, Dilarri G, Forsan CF, Sapata V de MR, Lopes PRM, de Moraes PB, Montagnolli RN, Ferreira H, Bidoia ED (2022b) Antibacterial action and target mechanisms of zinc oxide nanoparticles against bacterial pathogens. Sci Rep 12:2658. https://doi.org/10.1038/s41598-022-06657-y

Milaković M, Vestergaard G, González-Plaza JJ, Petrić I, Šimatović A, Senta I, Kublik S, Schloter M, Smalla K, Udiković-Kolić N (2019) Pollution from azithromycin-manufacturing promotes macrolide-resistance gene propagation and induces spatial and seasonal bacterial community shifts in receiving river sediments. Environ Int 123:501–511. https://doi.org/10.1016/j.envint.2018.12.050

Mohamed RM, Mkhalid IA, Baeissa ES, Al-Rayyani MA (2012) Photocatalytic Degradation of Methylene Blue by Fe/ZnO/SiO2 Nanoparticles under Visiblelight. J Nanotechnol 2012:329082. https://doi.org/https://doi.org/10.1155/2012/329082

Molla MAI, Furukawa M, Tateishi I, Katsumata H, Kaneco S (2020) Mineralization of Diazinon with nanosized-photocatalyst TiO2 in water under sunlight irradiation: optimization of degradation conditions and reaction pathway. Environ Technol 41:3524–3533. https://doi.org/10.1080/09593330.2019.1615129

Morejon B, Michel K (2023) A zone-of-inhibition assay to screen for humoral antimicrobial activity in mosquito hemolymph. Front Cell Infect Microbiol 13:891577. https://doi.org/10.3389/fcimb.2023.891577

Munzhelele EP, Mudzielwana R, Ayinde WB, Gitari WM (2024) Pharmaceutical Contaminants in Wastewater and Receiving Water Bodies of South Africa: A Review of Sources, Pathways, Occurrence, Effects, and Geographical Distribution. Water 16:796

Murray PR, Zeitinger JR (1983) Evaluation of Mueller-Hinton agar for disk diffusion susceptibility tests. J Clin Microbiol 18:1269–1271. https://doi.org/10.1128/jcm.18.5.1269-1271.1983

Navidpour AH, Abbasi S, Li D, Mojiri A, Zhou JL (2023) Investigation of Advanced Oxidation Process in the Presence of TiO2 Semiconductor as Photocatalyst: Property, Principle, Kinetic Analysis, and Photocatalytic Activity. Catalysts 13

Ortúzar M, Esterhuizen M, Olicón-Hernández DR, González-López J, Aranda E (2022) Pharmaceutical pollution in aquatic environments: a concise review of environmental impacts and bioremediation systems. Front Microbiol 13:869332

Pant B, Prasad Ojha G, Acharya J, Park M (2021) Ag3PO4-TiO2-Carbon nanofiber Composite: An efficient Visible-light photocatalyst obtained from electrospinning and hydrothermal methods.

Sep Purif Technol 276:119400. https://doi.org/https://doi.org/10.1016/j.seppur.2021.119400

Polianciuc SI, Gurzău AE, Kiss B, Ştefan MG, Loghin F (2020) Antibiotics in the environment: causes and consequences. Med Pharm reports 93:231–240. https://doi.org/10.15386/mpr-1742

Ranathunga K, Yapa P, Munaweera I, Weerasekera MM, Sandaruwan C (2024) Preparation and characterization of Fe–ZnO cellulose-based nanofiber mats with self-sterilizing photocatalytic activity to enhance antibacterial applications under visible light††Electronic supplementary information (ESI) available. See DOI: https://doi.o. RSC Adv 14:18536–18552. https://doi.org/https://doi.org/10.1039/d4ra03136a

Rezaei A, Katoueizadeh E, Zebarjad SM (2023) Investigating of the influence of zinc oxide nanoparticles morphology on the properties of electrospun polyvinyl alcohol/chitosan (PVA/CS) nanofibers. J Drug Deliv Sci Technol 104712

Rodríguez-López L, Santás-Miguel V, Núñez-Delgado A, Álvarez-Rodríguez E, Pérez-Rodríguez P, Arias-Estévez M (2022) Influence of pH, Humic Acids, and Salts on the Dissipation of Amoxicillin and Azithromycin Under Simulated Sunlight. Spanish J Soil Sci 12:10438

Ruziwa DT, Oluwalana AE, Mupa M, Meili L, Selvasembian R, Nindi MM, Sillanpaa M, Gwenzi W, Chaukura N (2023) Pharmaceuticals in wastewater and their photocatalytic degradation using nano-enabled photocatalysts. J Water Process Eng 54:103880. https://doi.org/https://doi.org/10.1016/j.jwpe.2023.103880

Sayadi MH, Homaeigohar S, Rezaei A, Shekari H (2021) Bi/SnO(2)/TiO(2)-graphene nanocomposite photocatalyst for solar visible light-induced photodegradation of pentachlorophenol. Environ Sci Pollut Res Int 28:15236–15247. https://doi.org/10.1007/s11356-020-11708-w

Sayadi MH, Sobhani S, Shekari H (2019) Photocatalytic degradation of azithromycin using GO@Fe3O4/ ZnO/ SnO2 nanocomposites. J Clean Prod 232:127–136. https://doi.org/https://doi.org/10.1016/j.jclepro.2019.05.338

Sharma M, Rajput D, Kumar V, Jatain I, Aminabhavi TM, Mohanakrishna G, Kumar R, Dubey KK (2023) Photocatalytic degradation of four emerging antibiotic contaminants and toxicity assessment in wastewater: A comprehensive study. Environ Res 231:116132. https://doi.org/https://doi.org/10.1016/j.envres.2023.116132

Shokri R, Jalilzadeh Yengejeh R, Babaei AA, Derikvand E, Almasi A (2019) Removal of azithromycin from wastewater using advanced oxidation processes (UV/H2O2) and moving-bed biofilm reactor (MBBR) by the response surface methodology (RSM). J Adv Environ Heal Res 7:249–259

Silva MJ, Soares SAR, Santos IDF, Pepe IM, Teixeira LR, Pereira LG, Silva LBA, Celino JJ (2020) Optimization of the photocatalytic degradation process of aromatic organic compounds applied to mangrove sediment. Heliyon 6:e05163. https://doi.org/https://doi.org/10.1016/j.heliyon.2020.e05163

Sirelkhatim A, Mahmud S, Seeni A, Kaus NHM, Ann LC, Bakhori SKM, Hasan H, Mohamad D

(2015) Review on Zinc Oxide Nanoparticles: Antibacterial Activity and Toxicity Mechanism. Nano-micro Lett 7:219–242. https://doi.org/10.1007/s40820-015-0040-x

Song L, Zhao F-Q, Xu S-Y, Ju X-H, Ye C-C (2020) Crystal Morphology Prediction and Anisotropic Evolution of 1,1-Diamino-2,2-dinitroethylene (FOX-7) by Temperature Tuning. Sci Rep 10:2317. https://doi.org/10.1038/s41598-020-59261-3

Song S, Wu K, Wu H, Guo J, Zhang L (2019) Effect of Fe/Sn doping on the photocatalytic performance of multi-shelled ZnO microspheres: experimental and theoretical investigations. Dalt Trans 48:13260–13272. https://doi.org/10.1039/C9DT02582K

Sosa-Hernández JE, Rodas-Zuluaga LI, López-Pacheco IY, Melchor-Martínez EM, Aghalari Z, Limón DS, Iqbal HMN, Parra-Saldívar R (2021) Sources of antibiotics pollutants in the aquatic environment under SARS-CoV-2 pandemic situation. Case Stud. Chem. Environ. Eng. 4:100127

Tiwari V, Mishra N, Gadani K, Solanki PS, Shah NA, Tiwari M (2018) Mechanism of Anti-bacterial Activity of Zinc Oxide Nanoparticle Against Carbapenem-Resistant Acinetobacter baumannii. Front Microbiol 9:1218. https://doi.org/10.3389/fmicb.2018.01218

Tong L, Eichhorn P, Pérez S, Wang Y, Barceló D (2011) Photodegradation of azithromycin in various aqueous systems under simulated and natural solar radiation: Kinetics and identification of photoproducts. Chemosphere 83:340–348

Wang Y, Liu Y, Qian Y, Lv L, Li X, Liu Y (2022) Characteristics of MgO/PCL/PVP antibacterial nanofiber membranes produced by electrospinning technology. Surfaces and Interfaces 28:101661. https://doi.org/https://doi.org/10.1016/j.surfin.2021.101661

Wang Y, Serrano S, Santiago-Aviles JJ (2003) Raman characterization of carbon nanofibers prepared using electrospinning. Synth Met 138:423–427

Wenhao Xiea, Yulin Shia, Yixuan Wanga, Yueling Zhenga, Hu Liub, Qian Huc, Suying Weid, Hongbo Gua, ∗ ZG (2021) Electrospun iron/cobalt alloy nanoparticles on carbon nanofibers towards exhaustive electrocatalytic degradation of tetracycline in wastewater. Chem Eng J 405:. https://doi.org/https://doi.org/10.1016/j.cej.2020.126585

Yang S, Wang W, Xu Y, Yuan Y, Hao S (2024) Fe-Zn alloy, a new biodegradable material capable of reducing ROS and inhibiting oxidative stress. Regen Biomater 11:rbae002. https://doi.org/10.1093/rb/rbae002

Yao L, Sun C, Lin H, Li G, Lian Z, Song R, Zhuang S, Zhang D (2023) Electrospun Bi-decorated BixTiyOz/TiO2 flexible carbon nanofibers and their applications on degradating of organic pollutants under solar radiation. J Mater Sci Technol 150:114–123. https://doi.org/https://doi.org/10.1016/j.jmst.2022.07.066

Yazdani A, Sayadi MH (2018) Sonochemical degradation of azithromycin in aqueous solution TT -. ehemj 5:85–92. https://doi.org/10.15171/EHEM.2018.13

Yu X, Zhang J, Zhang J, Niu J, Zhao J, Wei Y, Yao B (2019) Photocatalytic degradation of

ciprofloxacin using Zn-doped Cu2O particles: analysis of degradation pathways and intermediates. Chem Eng J 374:316–327

Zdainal Abidin SN, Lee HV, Asikin-Mijan N, Juan JC, Rahman NA, Mastuli MS, Taufiq-Yap YH, Kong PS (2020) Ni, Zn and Fe hydrotalcite-like catalysts for catalytic biomass compound into green biofuel. 92:587–600. https://doi.org/doi:10.1515/pac-2019-0820

Zhang W, Wang Y, Sun C (2007) Characterization on oxidative stabilization of polyacrylonitrile nanofibers prepared by electrospinning. J Polym Res 14:467–474

Zheng S, Wang Y, Chen C, Zhou X, Liu Y, Yang J, Geng Q, Chen G, Ding Y, Yang F (2022) Current Progress in Natural Degradation and Enhanced Removal Techniques of Antibiotics in the Environment: A Review. Int J Environ Res Public Health 19:. https://doi.org/10.3390/ijerph191710919

Zhou Z, Lai C, Zhang L, Qian Y, Hou H, Reneker DH, Fong H (2009) Development of carbon nanofibers from aligned electrospun polyacrylonitrile nanofiber bundles and characterization of their microstructural, electrical, and mechanical properties. Polymer (Guildf) 50:2999–3006

Supplementary Files

This is a list of supplementary files associated with this preprint. Click to download.

- Supplementarydata.docx